

Neutron spin manipulation optics: basic principles and possible applications

N K Pleshanov¹

Neutron Research Department, Petersburg Nuclear Physics Institute,
Orlova Roscha, Gatchina, St. Petersburg, 188300, Russia.

E-mail: pnk@pnpi.spb.ru

Abstract. A number of basic elements for neutron spin manipulation optics (NSMO) based on Larmor and non-Larmor (quantum) precessions under reflection are considered. It is concluded that transition to 3D in neutron polarization optics may bring additional instrumental possibilities. New neutron optical devices will include spin turners (particularly, $\pi/2$ -turners and π -turners, or flippers), spin precessors and antiprecessors, 3D-polarizers, 3D-analyzers, 3D-rotators, spin manipulators, hyper-polarizers. The innovative neutron optics is directly applicable to developing 3D polarization and polarimetry techniques, such as reflectometry with 3D-polarimetry, Neutron optical Spin Echo (NoSE), including compact NoSE and TOF NoSE schemes. A hyper-polarizer is a device which not only separates neutrons with the opposite spins, but also flips the ‘wrong’ spins. Thus, hyper-polarizers can double the intensity of polarized neutron beams, although a gain in the intensity can be achieved only with the increase either in the angular divergence or in the width of the beam, in full accordance with the Liouville theorem. The tasks to be solved for implementation of the NSMO concepts are discussed.

1. Introduction

Quantum mechanically, the neutron spin evolution is the result of superposition of the coherent spin states. Wherever the moduli of the opposite spin components do not change in time and space, the spin evolution may be described as precession. The quasi-classical Larmor precession picture and the quantum approach can be reconciled, when the spin-dependent scattering is negligible. Particularly, in a homogeneous magnetic medium both quasi-classical and quantum approaches lead to precession with the exactly Larmor frequency, even in the essentially non-classical case when the energies of the opposite spin components are different [1]. It is only when the neutron state is a superposition of non-orthogonal coherent states with different energies, the spin behavior in a homogeneous magnetic medium may have no classical counterpart [1,2].

In this paper we assume that polarized neutrons are prepared by stationary devices and the energies of the opposite spin components are equal. When the neutron with a mass m and a magnetic moment μ passes a distance l with the velocity $(v_+ + v_-)/2$ (t is the respective travel time) in a homogeneous magnetic medium, its spin turns (precesses) by an angle

$$\varphi_L = (k_- - k_+)l = (k_- - k_+) \frac{\hbar (k_+ + k_-)}{m} t = \omega_L t, \quad (1)$$

¹ To whom any correspondence should be addressed.



where $\omega_L = 2|\mu|B/\hbar$ is the Larmor frequency, $k_{\pm} = \sqrt{k^2 - \kappa_{\pm}^2}$ are the wave numbers, corresponding to the velocities v_{\pm} of the neutron in the states with the spin up (+) and down (−) the magnetic induction vector \mathbf{B} of the medium, $\kappa_{\pm} = \hbar^{-1}\sqrt{2m(V_n \pm V_m)}$ are the critical wave numbers of the medium with a nuclear potential V_n and the magnetic potential $V_m = |\mu|B$ for the (\pm) spin states; $k = \hbar^{-1}\sqrt{2mE}$, E is the neutron energy. Since $\mu < 0$, the neutron spin precession about \mathbf{B} is anticlockwise. In most cases $k \gg |\kappa_{\pm}|$, and one obtains

$$\varphi_L \cong l(\kappa_+^2 - \kappa_-^2)/k = ClB\lambda, \quad C = 8\pi m|\mu|/\hbar, \quad (2)$$

the well known law of proportionality ($C \cong 4.63 \cdot 10^5 \text{ T}^{-1}\text{m}^{-1}\text{nm}^{-1}$) of the precession angle to neutron path l [m], field magnitude B [T] and neutron wavelength λ [nm].

The orientation of the spin may be changed as a result of reflection from a layered structure with magnetic moments not collinear to the incident neutron spin. Thus, one can design magnetic structures that provide the required change of the spin direction.

For specular reflection of neutrons from a layered structure the Schrödinger equation is reduced to one-dimensional equation with the energy (θ is the glancing angle)

$$E_{\perp} = E \sin^2 \theta. \quad (3)$$

Its plane wave solutions for the incident and reflected neutrons are, respectively,

$$\Psi_0(z) = \begin{pmatrix} |\psi_0^+(z)| \cdot \exp[i\alpha_+(z)] \\ |\psi_0^-(z)| \cdot \exp[i\alpha_-(z)] \end{pmatrix}_Z, \quad \Psi_r(z) = \begin{pmatrix} |\psi_r^+(z)| \cdot \exp[i\beta_+(z)] \\ |\psi_r^-(z)| \cdot \exp[i\beta_-(z)] \end{pmatrix}_Z \quad (4)$$

(z is the surface normal coordinate, Z is the quantization axis).

Further we consider magnetically collinear layered structures and suppose the quantization axis Z to be parallel to their magnetization. If the spin-up and spin-down reflectivities differ ($R_+ \neq R_-$), the angle between the spin and Z changes. Therefore, it is only when $R_+ = R_-$, one may speak about precession of the spin under reflection. Then the orientation of the reflected neutron spin at the reflecting surface ($z = 0$) can be found by rotating the incident neutron spin about Z by an angle

$$\varphi = (\delta_- - \delta_+)_{z=0} = (\alpha_+ - \beta_+)_{z=0} - (\alpha_- - \beta_-)_{z=0}, \quad (5)$$

where δ_{\pm} are the shifts of the phases of the plane waves reflected in the (\pm) spin states relative to the phases of the incident waves in the same (\pm) spin state. The precession angle φ is defined so that it is positive for an anticlockwise (like Larmor) turn of the neutron spin. In order to observe the precession, the spins of the incident neutrons should be inclined to the direction of the magnetic fields in the reflecting layers. However, no one can guarantee now that it will be a Larmor precession.

Of interest for practical applications are the cases when the reflectivities from magnetic structures are close to 1. Then one may speak about neutron spin manipulation optics (NSMO). The possibility of building neutron spin turners on the basis of total reflection from magnetically anisotropic thin films has been mentioned in Ref. [3]. In the present paper the concepts of NSMO on the basis of magnetically collinear layered structures are developed. The magnetic moments are assumed to be in-plane and parallel to one another, although they may be inclined to sufficiently low external fields. It is justified in the first approximation, e.g., for numerous magnetic layers in remanent supermirrors [4-6] with the easy axis induced by sputtering conditions. Such coatings have been applied in remanent polarizers and analyzers [7]. Since low external fields do not affect the results noticeably, in further analysis the external fields are assumed to be absent. Numerical calculations are carried out with the *generalized matrix* method [8,9] (reinvented later under the name “*supermatrix* method” [10]).

2. Quantum precession of the neutron spin under total reflection

The precession condition is satisfied when neutrons in both spin states are totally reflected ($R_{\pm} = 1$). Consider precession under total reflection in the simplest cases.

2.1. Larmor precession coating (LPC)

First of all, consider total reflection of neutrons from a non-magnetic substrate coated with a magnetic film of thickness d , reflection from the upper boundary of which is negligible (figure 1). Taking account of the fact that the neutron traverses the magnetic film twice, before and after reflection from the substrate, the precession angle in terms of the wave vector transfer $q = 4\pi \sin(\theta)/\lambda$ (λ is the neutron wavelength, θ is the glancing angle) is

$$\varphi_L = qd \left[\sqrt{1 - (q_-/q)^2} - \sqrt{1 - (q_+/q)^2} \right] \quad (q \leq q_s), \quad (6)$$

where $q_{\pm} = 2\kappa_{\pm}$ are the critical wave numbers of the magnetic film for neutrons with the opposite spins. The condition $q \leq q_s = \hbar^{-1} \sqrt{2mV_s}$ corresponds to the inequality $E_{\perp} = E \sin^2 \theta \leq V_s$, i.e. to the condition of total reflection from the substrate with a potential V_s .

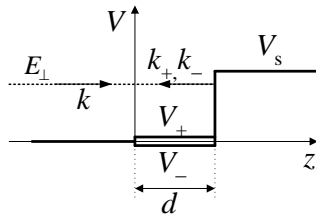


Figure 1. Total reflection of the neutron from a non-magnetic substrate in the presence of a weakly reflecting magnetic film (see details in the text).

Reflection from the upper boundary is negligible, when $q \gg |q_{\pm}|$. Then

$$\varphi_L \cong \frac{d(q_+^2 - q_-^2)}{2q} = 8\pi CB \frac{d}{q} = CB\lambda \frac{2d}{\sin \theta}. \quad (7)$$

This formula coincides with equation (2) for Larmor precession, since the length of the neutron path in the magnetic film is $l = 2d/\sin(\theta)$.

Such a magnetic coating that weakly reflects neutrons and induces Larmor precession will be called further as “Larmor precession coating” (LPC). Note that the precession angle is then proportional to the neutron path, B and λ , i.e. it decreases with q as q^{-1} .

Generally, definition (5) does not lead to Larmor precessions with the well-known relations. Consider two special cases of non-Larmor spin precessions, which are of interest from both conceptual and practical points of view.

2.2. Total reflection from the boundary with a magnetic medium

Reflection from the boundary with a magnetic medium has been considered in Ref. [11]. The simple formula derived [3] for the phase shift of the neutron wave under total reflection can be used to obtain the precession angle for the total reflection (TR) of both spin components from the boundary with a magnetic medium (figure 2-a):

$$\varphi_{TR} = 2[\arccos(q/q_+) - \arccos(q/q_-)] \quad (q \leq q_{\pm}). \quad (8)$$

The inequality $q \leq q_{\pm}$ is equivalent to $E_{\perp} \leq V_{\pm}$.

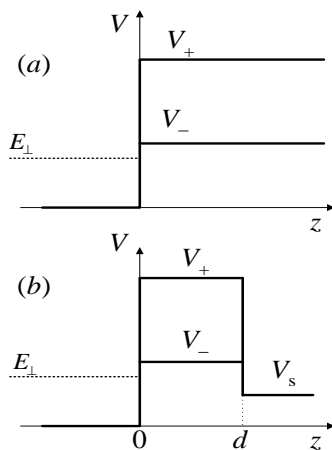


Figure 2. Total reflection of the neutron from the boundary with (a) a magnetic medium and (b) a thick magnetic film.

The precession is about the vector \mathbf{B} in magnetic medium, anticlockwise and increasing with q from 0 at $q = 0$ to a maximum $2\arccos(q_- / q_+)$ at $q = q_-$, so the precession angle can reach $\pi/2$ (when $V_+ \geq 2V_-$), but never can reach π . Note that the decrease of the precession angle with the wavelength corresponds with the fact that the neutron wave with a shorter wavelength penetrates deeper into the non-classical under-barrier region (with the field).

In practice, the precession is easier to observe [3,12] for reflection from a sufficiently thick magnetic film on a smooth substrate (figure 2-b). E.g., for an iron film thicker than 100 nm, the precession angle can be calculated with equation (8).

2.3. Total reflection with spin splitting

Even more peculiar precession is induced by spatial separation of the opposite spin components ('spin splitting'), which has been studied [13] and is exploited in NSE spectrometers [14] at J-PARC (Tokai, Japan).

When the spin-up and spin-down neutron components are totally reflected from different boundaries of a magnetic layer (the spin-down neutron reflection from its upper boundary is supposed to be negligible) with a thickness d and potential eigenvalues V_{\pm} (figure 3), the precession angle is

$$\varphi_s = qd\sqrt{1 - (q_- / q)^2} + (\varphi_{\text{TR}}^- - \varphi_{\text{TR}}^+) \quad (E_{\perp} \leq V_+, V_s), \quad (9)$$

i.e., it is defined by the phase difference related to different lengths of paths of neutron waves representing the states with the opposite spins as well as to the phase shifts $\varphi_{\text{TR}}^{\pm}$ under their total reflection from the respective boundaries:

$$\varphi_{\text{TR}}^+ = -2\arccos\sqrt{E_{\perp} / V_+}, \quad (10a)$$

$$\varphi_{\text{TR}}^- = -2\arccos\sqrt{(E_{\perp} - V_-) / (V_s - V_-)}. \quad (10b)$$

Account of the change in the kinetic energy and the relative height of the barrier for the spin-down neutron in the medium before the barrier (V_s) is taken in equation (10b).

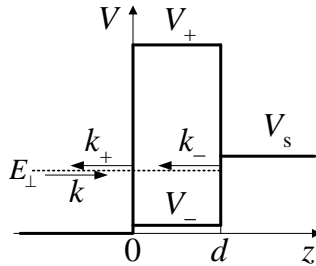


Figure 3. Total reflection with the spin splitting: the spin-up and spin-down neutron components undergo total reflection at the upper and lower interfaces of the magnetic film with a thickness d on a non-magnetic substrate with a potential V_s .

The precession is non-Larmor, anticlockwise for most parameters, but it can also be made clockwise ('antiprecession'), e.g. when $V_- = 0$ and $qd < \varphi_{\text{TR}}^+ - \varphi_{\text{TR}}^-$. However, when the total reflection conditions for the spin-up and spin-down components are identical ($V_+ = V_s$ and $V_- = 0$), the precession angle is positive and exactly proportional to q :

$$\varphi_s = qd = 4\pi d \sin(\theta) / \lambda. \quad (11)$$

As in the case of total reflection from the boundary with a magnetic medium, the non-classical behavior of the spin is related to purely quantum features of the interaction, in which the probabilities to find one and the same particle in the states with the opposite spins in a region with magnetic fields may essentially differ. Such interaction is impossible for a classical particle, which can be found at any time in a certain point and with a certain angular momentum.

3. Neutron spin manipulation optics: basic elements

Quantum aspects of the neutron interaction with magnetic layers open new possibilities for spin manipulations with neutron optical spin selectors, spin turners ($\pi/2$ - and π -turners, by way of example) and spin precessors. In order to analyze the potentialities of neutron spin manipulation optics, in fur-

ther calculations the magnetic layers are assumed to be homogeneously magnetized along the anisotropy axis, even when the external fields are switched off (perfect remanence).

3.1. Neutron optical spin selectors

All known neutron polarizers, including those on the basis of polarizing coatings, are spin selectors. Remanent polarizers can be magnetized in either of opposite directions thus eliminating the need of spin flippers [15,4] or can be rotated about their surface normals for polarized beam preparation and vector polarization analysis [16].

3.2. Neutron optical spin turners

Consider the possibility of building neutron spin turners on the basis of magnetically anisotropic thin films. The calculations are carried out for reflectors turning the spin by the angles $\pi/2$ and π , which are the most interesting for the practice. The task of rotation of the spin by any arbitrary angle is solved in the same manner.

The spin turner may be characterized by the orientation of the rotation axis and by the spin rotation angle γ . The efficiency of a spin turner can be defined as the portion of neutrons reflected with the spin in the desired direction \mathbf{u} , which is obtained by turning the incident beam polarization by the angle γ about the rotation axis, i.e.,

$$\varepsilon(\gamma) = (1 + P_u) / 2, \quad (12)$$

where P_u is the projection of the reflected beam polarization onto \mathbf{u} . Note that this is a generalization of the conventional definition of the efficiency of flippers. Further calculations are carried out on the assumption that the rotation axis is perpendicular to the incident neutron spin.

Curve 1 in figure 4-*a* is the precession angle φ calculated as a function of q in the region of total reflection of neutrons from a perfect boundary with magnetized bulk Fe. In practice, it is rather difficult to magnetize a bulk Fe to saturation and polish its surface to roughness about 1 nm. These problems are easily solved by using an Fe layer on a smooth substrate. For an Fe layer thicker 100 nm, the q -range of (almost) total reflection remains practically the same and the spin precession is described by curve 1. The use of a glass substrate with a sufficiently high potential ($V_s > V_-$) ensures total reflection even from an Fe layer as thin as 20 nm (curve 2). An Fe film, 100 nm or thicker, would be required with a silicon substrate ($V_s < V_-$). An oxide layer formed in air on the Fe layer surface sets up a barrier for neutrons and decreases the precession angle (curve 3).

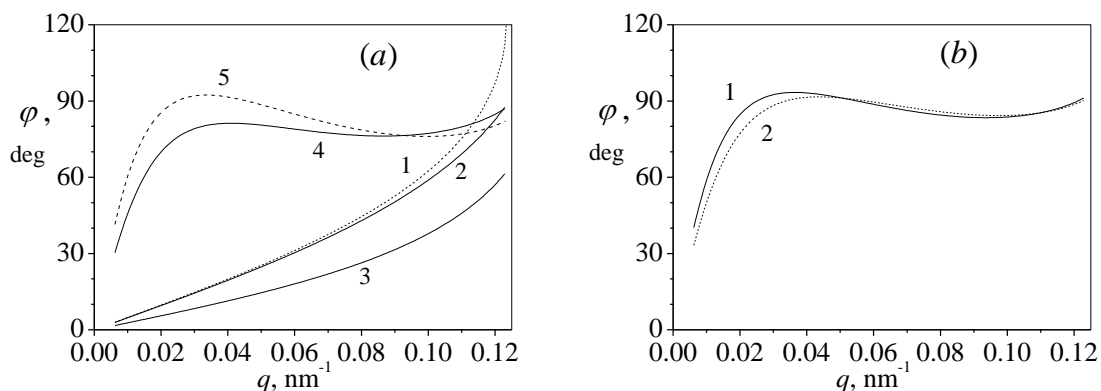


Figure 4. The precession angle φ calculated as a function of q in the total reflection region ($R_{\pm} = 1$) (a) from (1) magnetised bulk Fe ($V_n = 211$ neV, $V_m = 132$ neV); (2) Fe layer (20 nm); (3) Fe layer (20 nm) with a surface Fe_3O_4 (3 nm) oxide layer; (4) Fe layer coated with a Ti (15.5 nm) layer; (5) Fe layer (20 nm) coated with a Ti layer (20.5 nm) oxidized (TiO_2 3 nm) in air. (b) from an Fe layer (20 nm) coated with (1) TiH layer (14 nm, -65 neV), (2) TiH layer (16.5 nm, -60 neV) oxidized to TiO_2 (3 nm).

The layered structures are on the glass substrate ($V_s = 97$ neV).

As the precession angle essentially depends on q , spin turners based on total reflection from a single boundary with magnetic medium can work only with strongly collimated and monochromatic beams. So the ideas to relax these restrictions are required.

First, a layer with a negative potential V_b and an optimized thickness b (figure 5) can be used to form a medium before the total reflection boundary (*biased total reflection*). The phase shifts under biased total reflection from the barrier are defined by the kinetic energy $E_{\perp} - V_b$ and the barrier height $V_{\pm} - V_b$ in the medium before the barrier. As a consequence, the range of precession angles in the total reflection region decreases (cf. (10-a) and (10-b)). The precession is also affected by interference of the waves reflected from the boundaries of the additional layer and, optimizing its thickness b , one can additionally smoothen the dependence $\varphi(q)$ at the values of q , at which reflection from the upper boundary is still insignificant. Curve 4 in figure 4-a is for an Fe layer coated with a Ti layer; curve 5 represents the effect of its oxidation. The mean precession angle in the working q -range is somewhat below 90° , but it can be increased by hydrogenating titanium (figure 4-b).

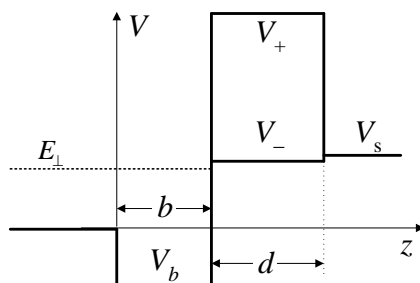


Figure 5. Total reflection of the neutron from the boundary with a thick magnetic film on the substrate.

The second idea boils down to balancing the non-Larmor precession (increasing with q) under reflection from the Fe layer with the Larmor precession (decreasing with q) in LPC on top of the Fe layer. One can use LPC made as a (multi)layer with a low (average) nuclear potential and comparatively low (average) magnetization to minimize reflection from its upper boundary. Curve 1 in figure 6 is calculated for LPC on the basis of a uniform layer with parameters optimized for a $\pi/2$ -turner and gives an example of the smoothing of the dependence $\varphi(q)$. The unfavorable effect of oxidation on the efficiency (curve 2) may be reduced to a considerable degree by depositing a thin Ti layer, which forms, due to oxidation in air, an *antireflection bilayer* Ti/TiO₂ [17,18] for neutrons (curve 3). The possibility of using a multilayer LPC, in which magnetic and non-magnetic thin layers are alternated (Co/Ti, Co/TiZr, CoFe/TiZr, etc.), is also confirmed by calculations. One must bear in mind this possibility in other examples of using LPC given below.

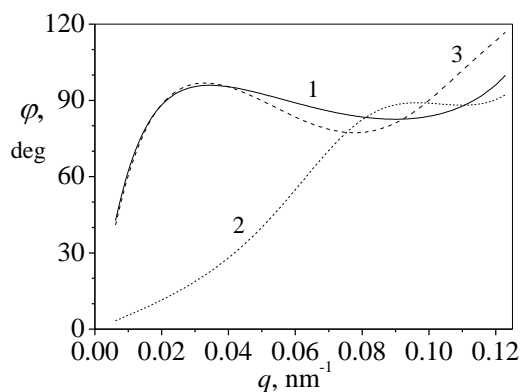


Figure 6. The precession angle φ calculated as a function of q in the region of total reflection from an Fe film (20 nm) coated with (1) LPC (35 nm, $V_n = -10$ neV, $V_m = 5.5$ neV); (2) LPC (40 nm, $V_n = 0$ neV, $V_m = 3$ neV) and a surface oxide (3 nm, 70 neV); (3) LPC (40 nm, $V_n = 0$ neV, $V_m = 3$ neV) and the bilayer Ti(5 nm)/TiO₂(3 nm). The layers are on the glass substrate ($V_s = 97$ neV).

The efficiencies of the $\pi/2$ -turners considered above are compared in figure 7. In all cases the effect of oxidation was taken into account. The thickness of the iron film is only 20 nm, because the glass substrate ensures total reflection of spin-down neutrons (V_s is even slightly above the potential of iron,

V_-). An Fe film with a thickness no less than 100 nm would be required with a silicon substrate ($V_s < V_-$). The mean efficiencies of all $\pi/2$ -turners in the working q -range from 0.02 to 0.123 nm^{-1} are above 0.99, so they can be of practical importance.

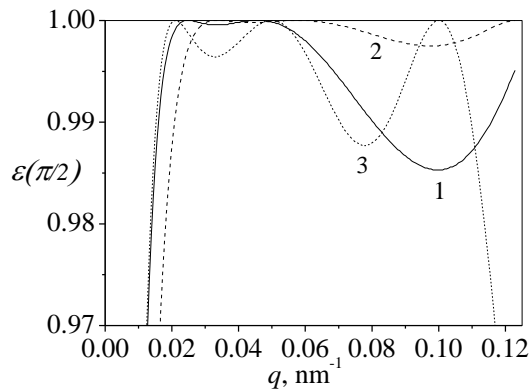


Figure 7. The efficiencies $\varepsilon(\pi/2)$ calculated as a function of q in the region of total reflection for the $\pi/2$ -turners on the basis of an Fe film (20 nm) coated with (1) Ti (20.5 nm) / TiO_2 (3 nm); (2) TiH (16.5 nm, -60 neV) / TiO_2 (3 nm); (3) LPC (40 nm, $V_n = 0$ neV, $V_m = 3$ neV) / Ti(5 nm)/ TiO_2 (3 nm). The efficiencies averaged in the q -range from 0.02 to 0.123 nm^{-1} are: (1) 0.9936, (2) 0.9987 and (3) 0.9923.

Performance of the spin turners may be improved by further optimization of the subsidiary layers and by combining the two approaches to smoothing the dependence $\varphi(q)$. However, the condition $E_\perp = E \sin^2 \theta \leq V_- = V_n - V_m$ for the total reflection of neutrons from the boundary with a medium with nuclear V_n and magnetic V_m potentials implies that the working glancing angles are very small. This is the chief drawback of such spin turners, so new ideas are required.

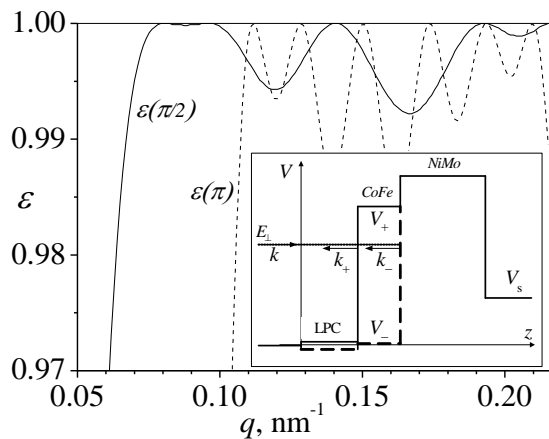


Figure 8. The efficiencies ε calculated as a function of q in the region of total reflection from spin-splitting structures and LPC. The solid curve is the efficiency of a $\pi/2$ -turner NiMo(100 nm) / CoFe (5 nm) / LPC (57 nm, $V_n = -10$ neV, $V_m = 10$ neV) / Ti(5 nm)/ TiO_2 (3 nm); the dotted curve is the efficiency of a π -turner NiMo(100 nm) / CoFe (10 nm) / LPC (130 nm, $V_n = -10$ neV, $V_m = 10$ neV) / Ti(5 nm)/ TiO_2 (3 nm). The mean efficiency of the $\pi/2$ -turner in the q -range from 0.075 to 0.215 nm^{-1} is 0.9976; the mean efficiency of the π -turner in the q -range from 0.11 to 0.215 nm^{-1} is 0.9948.

Inset: Neutrons in the spin-up and spin-down states experience total reflection from the LPC/CoFe and CoFe/NiMo (non-magnetic) boundaries, respectively. The spin-down neutron potential V_- of the magnetic layers is shown by the dashed lines. The Ti/ TiO_2 bilayer is not shown.

Not only $\pi/2$ -turners, but also π -turners can be built on the basis of spin-splitting structures. As before, we can use LPC to balance the non-Larmor precession. Since the spin-splitting structure may have a higher potential for total reflection of spin-down neutrons, the glancing angles for the spin turners can be increased. The mean efficiencies of such $\pi/2$ - and π -turners with optimized layers and an antireflective Ti/ TiO_2 bilayer also exceed 0.99 in the working q -ranges (figure 8).

What is more important, a magnetic LPC on top of a non-magnetic periodic multilayer may by itself induce the Larmor precession of the spins of the Bragg-reflected neutrons by any desired angle.

Due to small relative widths of the Bragg peaks, spin turners with record glancing angles and record efficiencies can be built. For a non-magnetic multilayer and a weakly reflecting LPC, the precession condition ($R_+ \equiv R_-$) is well satisfied. At the Bragg peak (large q), even layers of Co, Fe, or CoFe are weakly reflecting and can be used as LPC. In the examples given in figure 9 the averaged-over-the-peak efficiencies of the $\pi/2$ - and π -turners with the proper thicknesses of LPC exceed 0.999. When the period of the multilayer decreases, the Bragg peak width becomes lesser and the efficiency of the spin turner increases.

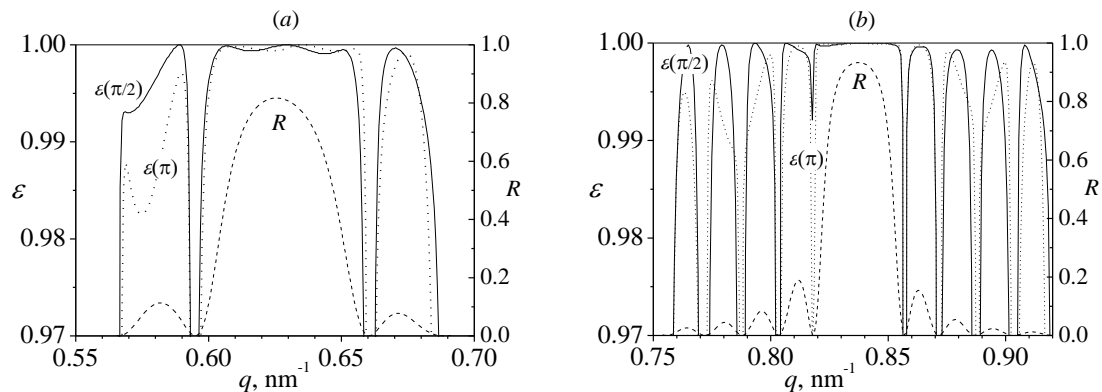


Figure 9. The reflectivities R and the efficiencies ε of the spin turners in the vicinity of the Bragg peak for non-magnetic multilayers (a) [NiMo(5.32nm)/Ti(4.94nm)]x20 and (b) [Ni-Mo(3.88nm)/Ti(3.73nm)]x50. The multilayers are coated with a Co layer of thickness (a) 46 nm and (b) 92 nm ($\pi/2$ -turners), and (a) 62 nm and (b) 123 nm (π -turners).

Earlier Zabel [19] has mentioned the possibility of using an antiferromagnetic (AF) superlattice as a flipper. When its magnetization is perpendicular to spins of incident neutrons, they are flipped within the Bragg magnetic reflection peak of $1/2$ order. Yet, it follows from calculations that the π -layers on non-magnetic multilayers are more efficient than AF superlattices; in addition, the efficiency of the AF superlattices as flippers decreases when their period diminishes. Still another advantage of the π -layers is a comparative ease of their production. Besides, spins of Bragg-reflected neutrons can be rotated by an arbitrary angle depending on the thickness of the magnetic layer (LPC).

The fact that rotation of neutron spins may be combined with the beam monochromatization is advantageous in some applications, but in most cases it will reduce the instrument luminosity. Therefore, consider the possibilities of producing spin turners on the basis supermirrors, which can reflect neutrons in the widest q -range (supermirrors with $m=7$ have been produced [20]).

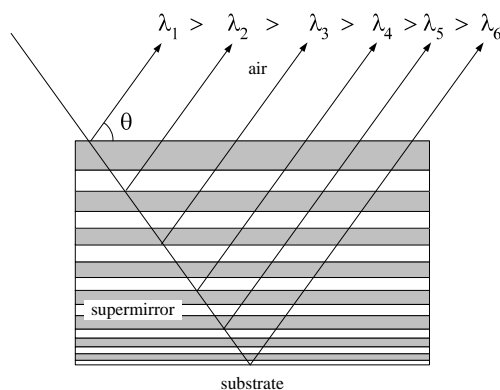


Figure 10. Reflected neutrons with lesser wavelengths traverse greater distances in the supermirror.

First of all, note that the path of neutrons reflected with larger q is longer, i.e. they traverse more layers, in the supermirror. It is illustrated in figure 10 for one glancing angle and different wave-

lengths. Reflection of neutrons with a given q is coherently enhanced at a group of bilayers with close-to-the-Bragg-condition thicknesses. Other bilayers are weakly reflecting and, if magnetic, induce Larmor precession. These features in neutron interaction can be used to design supermirror-based spin turners: neutrons reflected with larger q traverse more layers in the supermirror, and at the same time more magnetic layers are required to turn their spins by a given angle.

So, one approach is inclusion of magnetic layers into a non-magnetic supermirror. Thus, to build a $\pi/2$ -turner, Ti in 4 out of 300 NiMo/Ti bilayers was substituted by Co (in bilayers with numbers 1, 15, 77, 128 as counted from thicker ones), and a Co layer (7 nm) on top of the ($m=3$) supermirror was added (figure 11). 7 substitutions were made to build a π -turner. The efficiencies are moderate, but the method can certainly be developed by optimizing the parameters of the included magnetic layers.

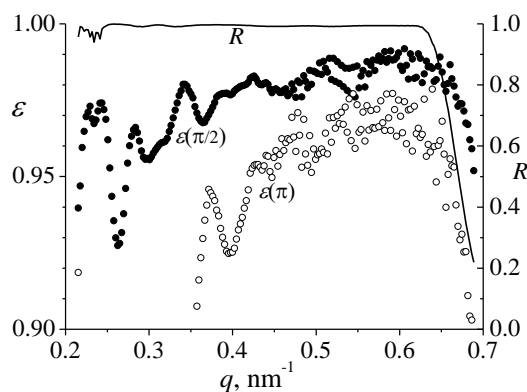


Figure 11. The reflectivities R and the efficiencies ε of spin turners on the basis of the NiMo/Ti ($m=3$) (300 bilayers) supermirror, in which some of the Ti layers are substituted by Co layers with the same thicknesses. An additional Co layer with a thickness 7 (14) nm is deposited on top of the $\pi/2$ (π)-turner. The points are obtained by convolution with the resolution $\Delta q/q = 0.03$.

Another approach is to use layers (uniform or composed of thinner layers of different materials) with low average magnetization. Calculations of the efficiencies of NiMo/X ($m=3$) $\pi/2$ - and π -supermirrors built with specially tuned magnetization of layers X are represented in figure 12. The material of the magnetic layers with required properties (see the neutron potentials in the caption) is designated as X; its elaboration is a task still to be solved. In principle, instead of Ti layers, NiMo layers could be substituted with magnetic layers, e.g., on the basis of Ni.

The efficiencies are good (Fig. 12), but only at larger q . Thicker bilayers function poorly. Removing 20 thicker bilayers, we can obtain very good efficiencies of $\pi/2$ - and π -turners at large q (figure 13-a). Still better efficiencies (exceeding 0.999) of the $\pi/2$ - and π -filters are obtained without 50 and 100 thicker bilayers (figure 13-b,c).

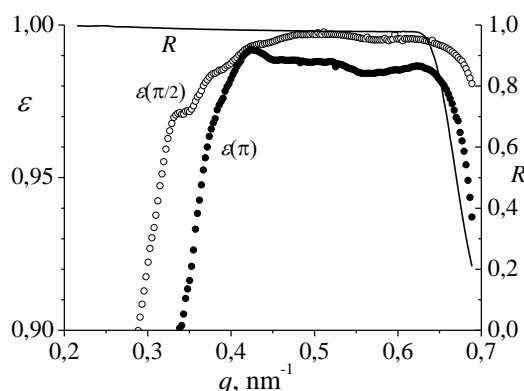


Figure 12. The reflectivities R and the efficiencies ε of spin turners on the basis of the NiMo/X ($m=3$) (300 bilayers) supermirror obtained from NiMo/Ti ($m=3$) sequence by substitution of Ti by X with the potentials $V_n = 0$, $V_m = 1.5$ neV ($\pi/2$ -turner) and $V_m = 3$ neV (π -turner). An additional Co layer with a thickness 26.5 (53) nm is deposited on top of the $\pi/2$ (π)-turner. The points are obtained by convolution with the resolution $\Delta q/q = 0.03$.

To design supermirror-based spin turners with high efficiency in the entire q -range, more sophisticated tuning of the parameters of magnetic layers is required. Particularly, the use of total reflection with the spin splitting essentially improves the efficiency of spin turners at low q .

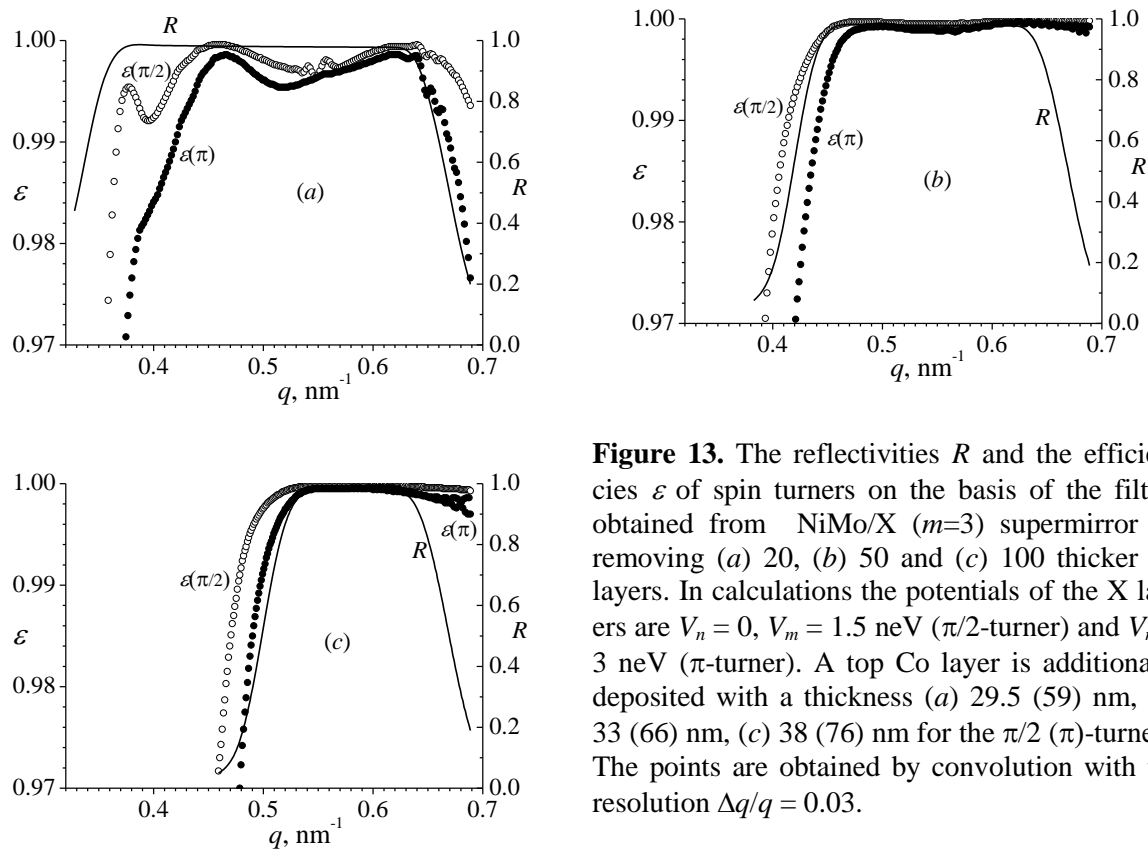


Figure 13. The reflectivities R and the efficiencies ε of spin turners on the basis of the filters obtained from NiMo/X ($m=3$) supermirror by removing (a) 20, (b) 50 and (c) 100 thicker bi-layers. In calculations the potentials of the X layers are $V_n = 0$, $V_m = 1.5$ neV ($\pi/2$ -turner) and $V_m = 3$ neV (π -turner). A top Co layer is additionally deposited with a thickness (a) 29.5 (59) nm, (b) 33 (66) nm, (c) 38 (76) nm for the $\pi/2$ (π)-turners. The points are obtained by convolution with the resolution $\Delta q/q = 0.03$.

3.3. Neutron optical spin precessors

Neutron optical spin precessors are spin turners designed to achieve large precession angles (analogue of precession coils used in the NSE arms). They may be characterized by the precession rate $|d\phi/dq|$ that defines the NSE length to be obtained when such precessors are placed in the NSE arms:

$$\rho_{\text{NSE}} = |d\phi/dq|. \quad (13)$$

In a quantum precessor developed in J-PARC (Tokai) a magnetic multilayer is stacked on top of a non-magnetic gap layer, which is above a non-magnetic multilayer, so that the spin-up and spin-down components reflect with a given q from different multilayers [21]. Multilayers on the basis of permalloy $\text{Fe}_{55}\text{Ni}_{45}$ are saturated in fields as low as 5 Oe. Multilayer quantum precessors have been applied in multilayer NSE [14] and multilayer interferometry [22].

We shall consider new possibilities related to using supermirrors. Two types of spin precessors can be envisaged: (1) Larmor precessors on the basis of LPC backed by a non-magnetic supermirror and (2) quantum precessors made as a stack of two supermirrors, each reflecting one of the spin components. We suppose that the condition $R_+ \cong R_-$ is fulfilled in both cases.

In the Larmor precessors a thick LPC, i.e. magnetic coating weakly reflecting neutrons in the working q -range, is deposited above a non-magnetic coating. Larmor precession of spins is induced when neutrons pass LPC before and after being reflected from the coating underneath. As an example, calculations of $|d\phi/dq|$ for a Co layer with a thickness 1 μm on top of a non-magnetic NiMo/Ti ($m=3$) supermirror are represented in figure 14. Curve 1 is calculated according to the formula

$$\left| \frac{d\phi_L}{dq} \right| \cong 8\pi C \frac{Bd}{q^2} \quad (14)$$

obtained from an approximate formula (7) for Larmor precessions under reflection. Account of a difference in the paths of neutrons with the opposite spins in the Co layer due to spin-dependent refrac-

tion has been taken in calculation of curve 2. The refraction correction becomes conspicuous for thick LPC and at small q . The exact numerical calculation of $|d\varphi/dq|$ (points) agrees with curve 2. In a NSE experiment with monochromatic neutrons, the ρ_{NSE} -scan can be made by changing the glancing angles. In TOF measurements the spatial correlation functions can be obtained simultaneously for a range of values of ρ_{NSE} . Note that the values of $|d\varphi/dq|$ in the working q -range are proportional to the LPC thickness, so the range of ρ_{NSE} can be optimized.

The scatter of points (Fig. 14) is related to differences in reflection of spin-up and spin-down neutron waves in the presence of the magnetic layer. Due to interference of the waves reflected at different interfaces and a large thickness of the magnetic layer, the resultant phase shifts are sensitive even to slight differences in the spin-up and spin-down neutron wave amplitudes. The scatter diminishes when the magnetization of LPC is reduced (with the proportional increase of its thickness). Thus, development of Larmor precessors suggests the use of materials with sufficiently low magnetization and sufficiently high remanence.

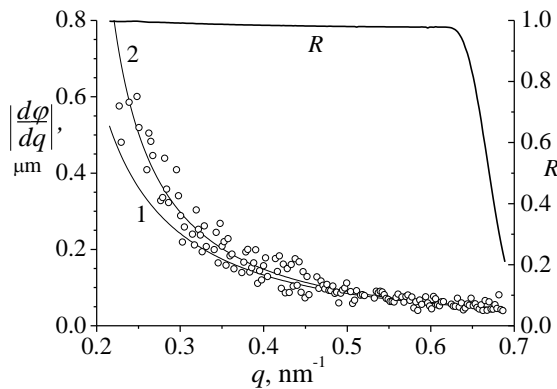


Figure 14. The precession rate $|d\varphi/dq|$ and the reflectivity R calculated for the Larmor precessor on the basis of a Co layer (1 μm) backed by the supermirror NiMo/Ti ($m=3$, 300 bilayers): (1) according to Larmor precession formula, (2) corrected for refraction, (o) exact numerical calculations.

Point out additional possibilities related to quantum precessors on the basis of supermirrors. First, by analogy with multilayers, consider using non-magnetic NiMo/TiZr supermirror (SM1) beneath and magnetic CoFe/TiZr supermirror (SM2) on top. The materials can be chosen so that $V_+(\text{CoFe}) = V(\text{NiMo})$ and $V_-(\text{CoFe}) = V(\text{TiZr}) = 0$. With the same sequence of thicknesses the equivalent layers in different supermirrors, reflecting the spin-up and spin-down neutrons with the same q , are always at a distance equal to the total thickness D of a supermirror. So $\varphi = Dq$, and $|d\varphi/dq| = D$ for any q , which is in agreement with numerical calculations (figure 15-a). The scatter of points is related to the discrete nature of the reflector now containing numerous magnetic layers with perfect interfaces.

Using a non-magnetic gap layer of thickness G between the supermirrors, one can change the precession rate to $|d\varphi/dq| = D+G$, or partly compensate a difference in the optical paths in SM1 and SM2, if any. Further we assume that $G = 0$.

The reflectivity R_+ of a real supermirror with rough interfaces may noticeably differ from 1, and spin-up neutrons will partly traverse through the magnetic supermirror and reflect from the non-magnetic supermirror. Calculations show that, as a consequence, not only the condition $R_+ \cong R_-$ is violated, but also the dependence $\varphi(q)$ is perturbed.

Perturbations due to unwanted reflections can be minimized when both supermirrors in the stack are magnetic, each reflecting one of the spin components. E.g., a CuTi/CoFe supermirror with $V(\text{CuTi}) = V_+(\text{CoFe})$ reflects only spin-down neutrons. It may be either beneath or on top of the CoFe/TiZr supermirror. It is in the first case that the spin splitting leads to precession with a minimum scatter of points (figure 15-b). (Multilayer precessors can also be improved in the same manner.) In the second case, the precession is in the opposite direction (antiprecession). Owing to refraction of the spin-up component in the CuTi/CoFe supermirror (the mean potential for this component is not equal to 0), the antiprecession rate depends on q (Fig. 15-b).

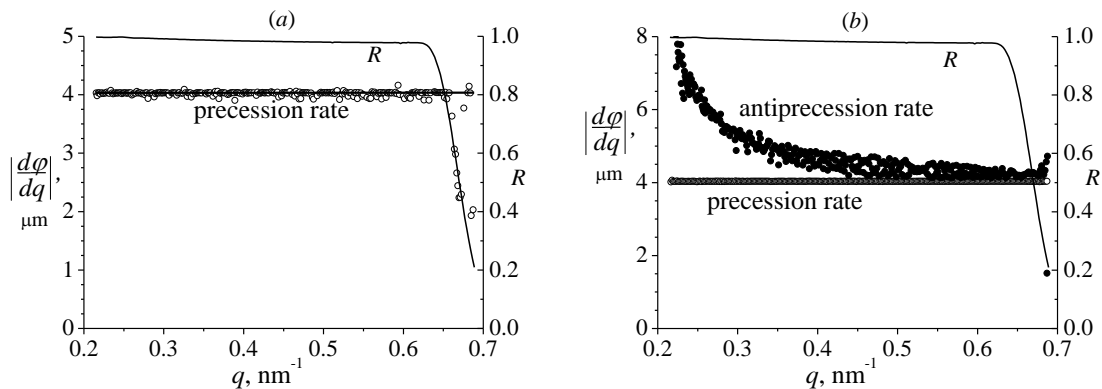


Figure 15. The precession rate $|d\phi/dq|$ and the reflectivity R calculated for the quantum precessor (a) on the basis of a CoFe/TiZr supermirror ($m = 3$, 300 bilayers) backed by a NiMo/Ti supermirror with the same sequence of thicknesses. The points (o) are exact numerical calculations, the solid line is the total thickness $D = 4.035 \mu\text{m}$ of a supermirror; (b) on the basis of a stack of CoFe/TiZr and CuTi/CoFe supermirrors with the same sequence ($m = 3$), the CuTi/CoFe supermirror being either beneath (o) or on top (\bullet).

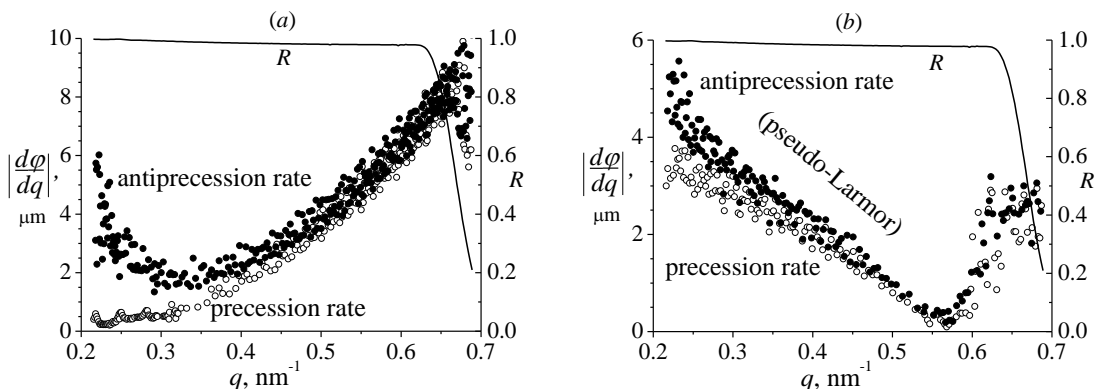


Figure 16. The precession rate $|d\phi/dq|$ and the reflectivity R calculated for the quantum precessor on the basis of CoFe/TiZr ($m = 3$) и CuTi/CoFe ($m = 3$) supermirrors with inverted sequence of thicknesses of (a) the upper and (b) the lower supermirror, when the CuTi/CoFe supermirror is beneath (o) and on top (\bullet).

Spin precessors with a constant rate $|d\phi/dq|$ can be used in NSE experiments with beams of large divergence or/and wide wavelength band. A set of quantum precessors with different D would be required to measure the spatial correlation function. In principle, one may use external fields to scan near discrete values of ρ_{NSE} .

Inverting the sequence of thicknesses (thinner bilayers above thicker ones) in one of the supermirrors, one can introduce dependence of $|d\phi/dq|$ on q . The distance between the equivalent layers increases (decreases) with q , when the sequence of the upper (lower) supermirror is inverted. Correspondingly, precession and antiprecession rates will be increasing (decreasing) with q (Fig. 16). The phases of the neutron waves reflected from initial and inverted sequences of the equivalent layers are different, even when the reflectivities are the same. It explains the non-monotonic behavior of $|d\phi/dq|$ as a function of q . Precession and antiprecession with $|d\phi/dq|$ that decreases with q may be called pseudo-Larmor. The dependences of $|d\phi/dq|$ on q may be corrected by means of gap layers.

4. Innovative neutron optics instrumentation

NSMO basic elements have been considered. It has been concluded that some elements can work with beams of neutrons with wide wavelength band and large divergence. Combining the NSMO elements, one can design innovative neutron optics instrumentation. Rotation of NSMO elements about their reflecting surface normals may bring additional instrumental possibilities. Magnetic screens can be used to eliminate external fields for the efficient work of NSMO devices. Since the elements are based on very thin coatings, the polarized neutron devices can be made quite compact.

4.1. Neutron 3D polarizers

Using a spin-selector followed by a $\pi/2$ -turner, we can build a 3D polarizer producing beams with polarization in any desired direction from an initially unpolarized beam. A scheme of the 3D polarizer is represented in figure 17. Note that the design with the reflecting surface on the opposite side is also possible.

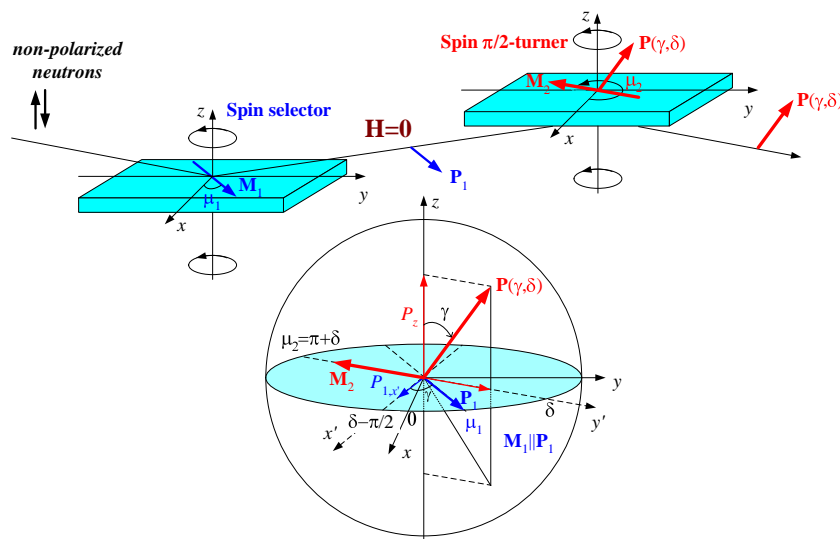


Figure 17. Scheme of a (broad band) 3D polarizer and its theory. The spin selector and the $\pi/2$ -turner can be rotated about their reflecting surface normals. For the sake of visibility, the magnetization \mathbf{M}_2 of the $\pi/2$ -turner coating is drawn on the back side of the substrate.

The reflecting surfaces of the spin-selector and the $\pi/2$ -turner are assumed to be parallel to each other and coincide with the equatorial plane of the unitary sphere (figure 17). The z -axis is along the normal to the reflecting surfaces, so the x -axis and the y -axis are in the equatorial plane. Define the desired polarization vector \mathbf{P} by the polar angle δ of its projection onto the equatorial plane and by its tilt γ relative to the z -axis. The angle δ is counted from the x -axis to the y -axis.

Designate the direction of the projection of the vector \mathbf{P} onto the equatorial plane as y' and introduce the x' -axis in this plane. By definition, the direction of y' is defined by the angle δ . The polarization vector \mathbf{P}_1 after the spin selector is in the equatorial plane. Rotation of \mathbf{P}_1 about the y' -axis by $\pi/2$ leaves the component $P_{1,y'}$ unchanged, and aligns the component $P_{s,x'}$ along the z -axis. Provided that $P_{1,x'} = P_z = \cos\gamma$, we obtain the vector \mathbf{P} with the preset angles δ and γ . In the coordinates (x', y') the vector $\mathbf{P}_1 = (\cos\gamma, \sin\gamma)$, so in the coordinates (x, y) its direction is defined by the polar angle

$$\mu_1 = \gamma - (\pi/2 - \delta) \quad (15)$$

(see also figure 17). Since $\mathbf{P}_1 \parallel \mathbf{M}_1$, μ_1 is the angle for the magnetization of the spin selector. Taking account of the sign of precession, the magnetization of the $\pi/2$ -turner should be opposite to the y' -axis (figure 17), i.e.

$$\mu_2 = \pi + \delta. \quad (16)$$

Therefore, the 3D-polarizer can form a neutron beam with any direction of the polarization $\mathbf{P}(\delta, \gamma)$, provided that the spin selector and the $\pi/2$ -turner can be rotated about their surface normals.

3D-polarizers for preparation of monochromatic beams can be made more compact (figure 18), when a substrate transparent for neutrons (silicon, quartz, etc.) with LPC is placed immediately above the polarizing multilayer. An unpolarized beam, after traversing the transparent substrate and LPC, is monochromatized and polarized in the multilayer; being reflected from the multilayer, the polarized beam passes through LPC with magnetization and thickness optimized for turning spins by $\pi/2$ (note that the polarized neutrons pass LPC only once). With independent rotations of the substrates about their surface normals, any preset direction of the polarization $\mathbf{P}(\delta, \gamma)$ of the monochromatic beam is achieved with the magnetizations of the polarizing multilayer and the $\pi/2$ -LPC at angles (15) and (16), respectively.

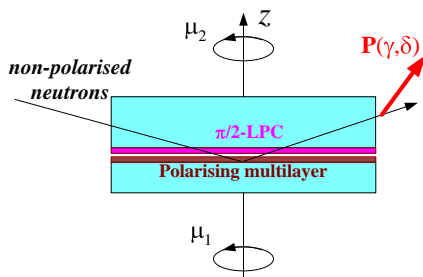


Figure 18. Scheme of a compact 3D polarizer for producing monochromatic beams with polarization in any desired direction. The two substrates can be rotated independently to align magnetizations of the polarizing multilayer and the $\pi/2$ -LPC spin turner in the directions required.

4.2. Neutron spin 3D rotator

A π -turner followed by a $\pi/2$ -turner can work as a 3D rotator (figure 19), rotating spins from any direction $\mathbf{P}_0(\delta_0, \pi/2)$ in the reflecting plane to any desired direction $\mathbf{P}(\delta, \gamma)$. The theory of the 3D rotator is similar to that of the 3D polarizer. First, we can rotate \mathbf{P}_0 in the equatorial plane from δ_0 to the angle $\delta_1 = \gamma - (\pi/2 - \delta)$ by directing the magnetization of the π -turner at the angle

$$\mu_1 = (\delta_0 + \delta_1)/2 = [(\delta_0 + \delta) + (\gamma - \pi/2)]/2. \quad (17)$$

With the magnetization of the $\pi/2$ -turner at the angle μ_2 given by (16), we obtain the reflected beam with the desired polarization $\mathbf{P}(\delta, \gamma)$. A more detailed analysis shows that there are four pairs of μ_1 and μ_2 that produce the same result. The magnetizations at $\mu_1 = [(\delta_0 + \delta) - (\gamma - \pi/2)]/2$ and $\mu_2 = \delta$ would also transfer $\mathbf{P}_0(\delta_0, \pi/2)$ to $\mathbf{P}(\delta, \gamma)$. The other pairs are obtained by substituting $\mu_1 + \pi$ for μ_1 in the first two combinations.

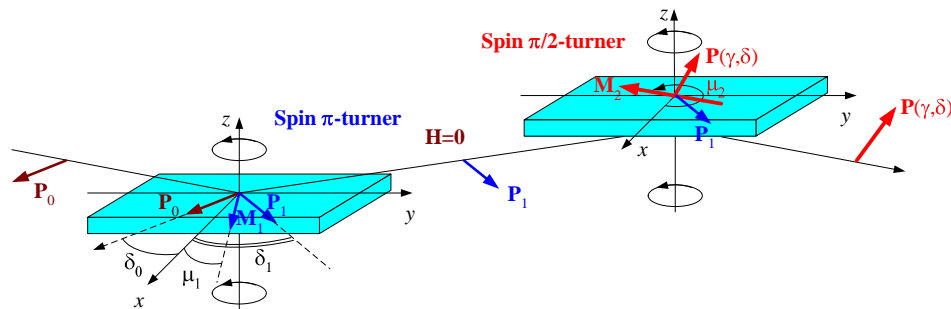


Figure 19. Scheme of a (broad band) 3D rotator. The π -turner and the $\pi/2$ -turner can be rotated about their reflecting surface normals.

4.3. Neutron spin manipulator.

Adding a $\pi/2$ -turner before the π -turner in the scheme in figure 18, one can rotate spins from any direction to any direction (figure 20). The additional $\pi/2$ -turner is needed to rotate spins from an initial direction $\mathbf{P}_0(\delta_0, \gamma_0)$ into the reflecting plane. Therefore, its magnetization should be at the angle δ_0 (or $\delta_0 + \pi$), i.e. along the projection of \mathbf{P}_0 onto the reflecting plane. Then the polarization vector of neu-

trons reflected from the first $\pi/2$ -turner will be in the reflecting plane at an angle δ_1 . And the task is reduced to the one considered in section 4.2.

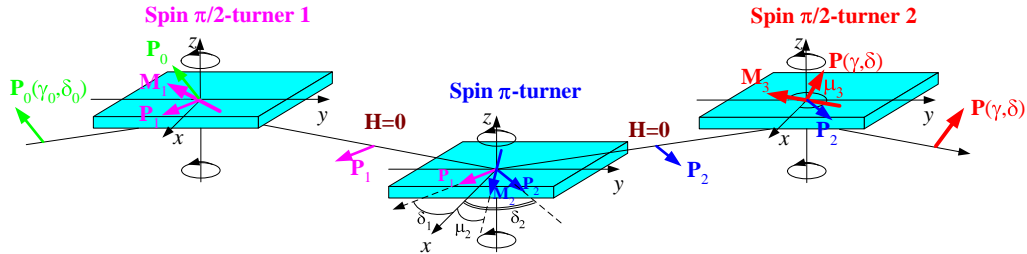


Figure 20. Scheme of a (broad band) spin manipulator. All spin turners can be rotated about their reflecting surface normals.

4.4. Neutron 3D analyzers

A new possibility of measuring three components of the polarization vector is also to be mentioned. First, two polarization components in the reflecting plane of a spin selector are measured by rotating it about its surface normal and finding intensities for four orientations of its magnetization. Then, introducing a $\pi/2$ -turner before the spin selector (inverting the scheme of the 3D polarizer in figure 17), one can measure the polarization component perpendicular to the reflecting plane of the spin selector. It suffices to measure intensities for opposite magnetizations of either $\pi/2$ -turner or spin selector. For monochromatic beams, a $\pi/2$ -LPC spin turner can be placed above the spin selector, as shown in figure 18. An even more distinct solution would be a polarizer coated by a $\pi/2$ -LPC, with their magnetizations being perpendicular.

4.5. Neutron hyper-polarizers

Common polarizers are conceived as spin selectors transmitting neutrons with the desired spin (50%) and eliminating neutrons with the ‘wrong’ spin (50%). Define a hyper-polarizer as a device which not only separates neutrons with the opposite spins, but also flips the wrong spins, thus polarizing more than 50% (up to 100%) of neutrons. A gain in polarized neutron intensity can be achieved only with the increase either in the angular divergence (hyper-polarizers of type I) or in the width (hyper-polarizers of type II) of the beam, so that the total phase volume doubled by the spin subspace is conserved (the Liouville theorem).

4.5.1. Hyper-polarizers of type I. Two variants of the scheme of a hyper-polarizer of type I are represented in figure 21. The polarizing filter on the basis of a periodic multilayer (or truncated supermirror) reflects only spin-up neutrons in the range from $q_{\min}^+ = 4\pi \sin \theta_{\min}^+ / \lambda_{\max}$ to $q_{\max}^+ = 4\pi \sin \theta_{\max}^+ / \lambda_{\min}$. The extreme angles and wavelengths in the formulas are defined by mean glancing angle θ_+ and beam divergence $\Delta\theta$, as well as by mean wavelength and wavelength band width. The spin-down neutrons traverse the polarizing filter and reflect from a spin-flipping π -coating (flipper). The reflecting surface of the flipper is turned relative to the filter surface by an angle α . The angle α is chosen so that neutrons with flipped spins traverse the filter without being reflected:

$$\alpha > \theta_{\max}^+ \frac{\lambda_{\max}}{\lambda_{\min}} - \theta_{\min}^+. \quad (18)$$

The reflection q -range of the flipper should include the interval from $q_{\min}^- = 4\pi \sin(\theta_{\min}^+ + \alpha) / \lambda_{\max}$ to $q_{\max}^- = 4\pi \sin(\theta_{\max}^+ + \alpha) / \lambda_{\min}$. Condition (18) is obtained on the assumption that all glancing angles are small; more generally, the flipper coating and the angle α must provide that $q_{\min}^- > q_{\max}^+$.

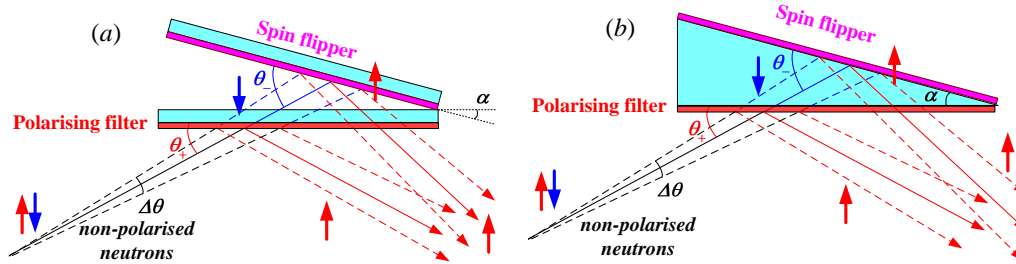


Figure 21. Schemes of a hyper-polarizer of type I: (a) angle design and (b) wedge design.

The spin-up neutron reflectivity of the polarizing filter should be close to 1, since spin-up neutrons passing through the filter are reflected from the flipper with the “wrong” spin. E.g., for the polarizing filter one could use a thick CoFe film totally reflecting spin-up neutrons at the glancing angles below the critical angle and transmitting spin-down neutrons. Being reflected from a multilayer flipper, neutrons should traverse the CoFe film at glancing angles exceeding the critical angle.

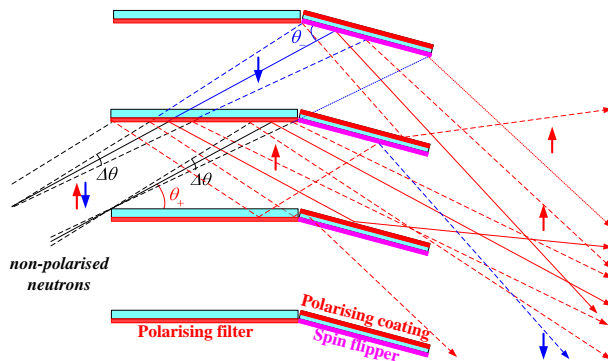


Figure 22. Multichannel design of a hyper-polarizer of type I.

Other conditions for hyper-polarization of neutron beams are also possible, the main requirement being that neutrons reflected from the flipper either traverse through ($\theta > \theta_+$) or miss (it is possible when schemes in figure 21 are inverted, i.e. $\theta < \theta_+$) the polarizing filter. To intercept a wide beam, one can build a hyper-polarizer from several hyper-polarizing angles (wedges) or use a multichannel design (figure 22). Hyper-polarizers of type I are fit for hyper-polarization of collimated monochromatic beams.

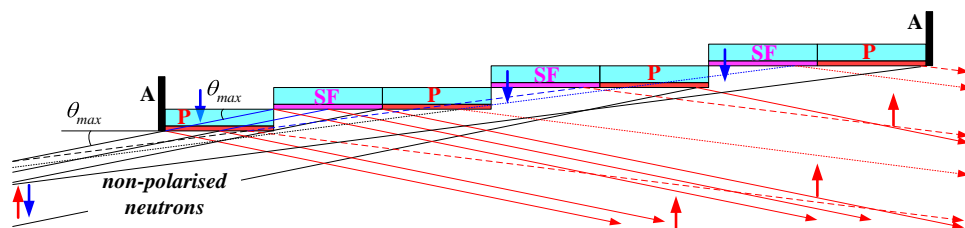


Figure 23. Scheme of a hyper-polarizer of type II (hyper-polarizing staircase): P=polarizing coating, SF=spin-flipping coating, A=neutron absorber.

4.5.2. Hyper-polarizers of type II. To hyper-polarize broad-band neutron beams, one can use a hyper-polarizing staircase built from hyper-polarizing steps as shown in figure 23. For glancing angles below the diagonal angle $\theta_{\max} = \arctan(h/L_p)$, where h is the step height and L_p is the length of the substrate (wafer) with a polarizing coating (P), the spin-up neutrons are reflected from the polarizing coatings, and the spin-down neutrons traverse the polarizing coatings until they are reflected from a spin-flipping π -coating (SF). As a consequence, the reflected beam is hyper-polarized.

4.5.3. Additional possibilities for hyper-polarization. Mention two additional possibilities. The first is the scheme of a hyper-polarizer which has been suggested earlier [16] and allows of hyper-polarizing a broad-band neutron beam without spin-flip reflection. The spin-up neutrons are reflected from a polarizing coating on top of a layered structure with a gradually rotating magnetization, in which spins of transmitted neutrons reverse adiabatically. The scheme became realizable after a publication by Kraan and Rekvelde [23] on the possibility of using a single domain wall in a permalloy film as a neutron spin flipper.

Secondly, an unpolarized beam can be split into sub-beams with the opposite spins not only by reflection, but also by spin-dependent refraction, e.g. between two sharp magnetic poles (Stern-Gerlach splitting). Reflecting one of the sub-beams from a neutron optical π -turner, one can achieve hyper-polarization. Moreover, moving the π -turner from one sub-beam to the other is equivalent to using a flipper.

4.6. Double-reflection spin turners

All rays reflected consequently from two mirrors with reflecting surfaces at an angle β to each other (periscope geometry in Fig. 24) are deviated by the same angle:

$$2(\beta_1 + \beta_2) = 2\beta, \quad (19)$$

where β_1 and β_2 are the glancing angles of reflection from mirrors 1 and 2, accordingly. It means that layered structures that produce spin precession by angles proportional to q , i.e. to the glancing angle θ ($\sin\theta \cong \theta$ for thermal and cold neutrons), can be used to build spin turners for monochromatic beams. According to (19), spins of all monochromatic neutrons consequently reflected from two identical spin turners based on spin-splitting coatings will be rotated by one and the same angle

$$\varphi = 4\pi\beta D/\lambda, \quad (20)$$

which depends on neutron wavelength λ , spin-splitting distance D and angle β . In particular, for a certain wavelength it can be made $\pi/2$ and π (figure 24).

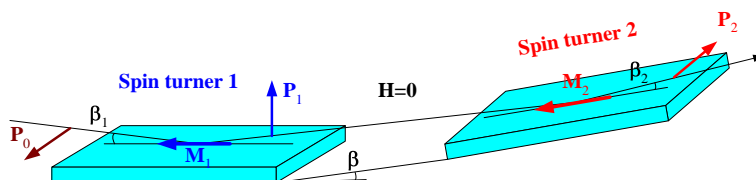


Figure 24. Scheme of a double-reflection spin flipper. Two identical $\pi/2$ -turners are based on spin-splitting coatings.

4.7. Multichannel spin turners.

Multichannel design of spin turners is possible, provided that the number of reflections from the spin-turning coatings in each channel can be fixed (say, reduced to 1, when one of the channel walls is weakly reflecting and absorbs neutrons). Combining a multichannel $\pi/2$ -turner with a multichannel analyzer, one could measure at least two neutron polarization vector components.

5. Discussion

The existing polarized neutron optics is built on the basis of polarizing coatings that work as spin selectors. A variety of elements for neutron spin manipulation optics (NSMO) based both on Larmor and non-Larmor precession under reflection has been considered. It can be concluded that transition to 3D in neutron polarization optics brings additional instrumental possibilities. New neutron optical devices may include spin turners (particularly, $\pi/2$ -turners and π -turners, or flippers), spin precessors and anti-precessors, 3D-polarizers, 3D-analyzers, 3D-rotators, spin manipulators, hyper-polarizers. Possible applications of the innovative neutron optics range from 3D polarization and polarization analysis to new neutron optics instrumentation. Hyper-polarizers can double the intensity of polarized neutron beams. In accordance with the Liouville theorem, a gain in intensity can be achieved only with the increase either in the angular divergence (hyper-polarizers of type I) or in the width (hyper-polarizers

of type II) of the beam. However, hyper-polarizers of type I can be focused onto the sample. It is easier to transport a neutron beam with a lower cross section and then polarize it with a hyper-polarizer of type I or II. Besides, neutron beams at the outlets of the existing neutron guides can be hyper-polarized to achieve a gain in the polarized neutron intensity. Another strategy is to place a hyper-polarizer in front of the conventional polarizer to achieve a gain in both intensity and polarization of the beam. The possibility to build a hyper-polarizer by sputtering a polarizing coating onto a permalloy film, the thickness of which is optimum for formation of single domain walls, is also worth studying. Hyper-polarization of a Stern-Gerlach-split beam with a π -turner might also be of interest in some applications.

NSMO is directly applicable to developing such techniques as reflectometry with 3D-polarimetry for both monochromatic and white neutron beams, Neutron optical Spin Echo (NoSE), including compact NoSE and TOF NoSE schemes, based only on neutron optical devices ($\pi/2$ -turners, π -turners and precessors). Development of polarimetry with VCN and even UCN on the basis of the neutron optical spin turners is a challenge that can now be addressed. UCN polarimetry is an equivalent of ellipsometry, but with extreme sensitivity to surface magnetism. New UCN sources and progress with NSMO may allow of developing this technique.

NSMO can be made broad-band, which is of special interest for applications at impulse reactors and spallation sources. As the working parts of NSMO are very thin coatings, the devices can be made quite compact and used, e.g., for handling micro-beams [24,25].

The potential of the innovative optics is still to be revealed by studies of spin precession phenomena with real structures. Coercivity and remanence of coatings on the basis of magnetic layers are of decisive importance. Surface oxidation is also to be addressed as an important issue for the work of the spin turners. The magnetic layers for spin turners are too thin to produce significant stray fields. However, stray fields from numerous magnetized layers of remanent supermirrors in the absence of the guide field may detectably rotate the neutron polarization vector [12]. Efficient ways of compensating stray fields have been proposed and substantiated by numerical calculations in Ref. [12]. They may be needed and can be developed for supermirror-based spin selectors and spin precessors. Numerous problems may be envisaged in developing spin precessors based on Larmor and non-Larmor spin precessions under reflection from magnetic layered structures. Step by step approach is required to find appropriate solutions.

Acknowledgements

The work was partly supported by RFBR grant No. 12-02-12066-ofi_m.

References

- [1] Pleshanov N K 2001 *Physica B* **304** 193
- [2] Pleshanov N K 2000 *Phys. Rev. B* **62** 2994
- [3] Pleshanov N K 1994 *Physica B* **198** 70
- [4] Böni P, Clemens D, Kumar M Senthil, Pappas C 1999 *Physica B* **267-268** 320
- [5] Pleshanov N K, Bodnarchuk V, Gähler R, Korneev D A, Menelle A, Metelev S V, Pusenkov V M, Schebetov A F, Ul'yanov V A 2001 *Physica B* **297** 126
- [6] Kumar M Senthil, Böni P 2002 *J. Appl. Phys.* **91** 3750
- [7] Pappas C, Kali G, Krist T, Böni P, Mezei F 2000 *Physica B* **283** 365
- [8] Pleshanov N K 1996 *Z. Phys. B* **100** 423
- [9] Pleshanov N K, Pusenkov V M 1996 *Z. Phys. B* **100** 507
- [10] Rühm A, Toperverg B P, Dosch H 1999 *Phys. Rev. B* **60** 16073
- [11] Pleshanov N K 1994 *Z. Phys. B* **94** 233
- [12] Pleshanov N K, Axel'rod L A, Zabenkin V N, Syromyatnikov V G, Ul'yanov V A 2008 *J. Surface Investigation* **2** 846
- [13] Ebisawa T, Tasaki S, Kawai T, Hino M, Achiwa N, Otake Y, Funahashi H, Yamazaki D, Akiyoshi T 1998 *Phys. Rev. A* **57** 4720

- [14] Tasaki S, Ebisawa T, Maruyama R, Achiwa N, Kawai T, Kawabata Y, Hino M, Yamazaki D 2003 *Physica* **B 335** 234
- [15] Korneev D A 1992 *Neutron Optical Devices and Applications: Proc. SPIE* vol 1738, ed C F Majkrzak, J L Wood p 477
- [16] Pleshanov N K 2001 *Physica* **B 297** 131
- [17] Pleshanov N K 2010 *Nucl. Instrum. Methods* **A 613** 15
- [18] Matveev V A, Pleshanov N K, Bulkin A P, Syromyatnikov V G 2012 *J. of Physics: Conf. Ser.* **340** 012086
- [19] Zabel H 1994 *Physica* **B 198** 156
- [20] <http://www.swissneutronics.ch>
- [21] Funahashi H, Ebisawa T, Haseyama T, Hino M, Masaike A, Otake Y, Tabaru T, Tasaki S 1996 *Phys. Rev.* **A 54** 649
- [22] Hino M, Achiwa N, Tasaki S, Ebisawa T, Kawai T, Yamazaki D 2000 *Phys. Rev.* **A 61** 136071
- [23] Kraan W H and Rekveldt M T 2008 *Nucl. Instrum. Methods* **A 596** 422
- [24] Kozhevnikov S V, Rühm A, Ott F, Pleshanov N K, Major J 2011 *Physica* **B 406** 2463
- [25] Rühm A, Kozhevnikov S V, Ott F, Radu F, Major J 2013 *Nucl. Instrum. Methods* **A 708** 83